AGU PUBLICATIONS

Space Weather

RESEARCH ARTICLE
10.1002/2016SW001582

Key Points:
- Variations of midlatitudinal atmospheric and space weather parameters are compared
- Temperature and pressure at 250-30 hPa levels found to anticorrelate with the cosmic ray flux
- The anticorrelation can be caused both by a dynamical coupling between the middle and high latitudes and by a local "atmospheric effect"

Supporting Information:
- Supporting Information S1

Correspondence to:
A. L. Morozova,
annamorozovauc@gmail.com

Citation:
Morozova, A. L., J. J. Blanco, and P. Ribeiro (2017), Modes of temperature and pressure variability in midlatitude troposphere and lower stratosphere in relation to cosmic ray variations, *Space Weather*, *15*, 673–690, doi:10.1002/2016SW001582.

Received 5 DEC 2016
Accepted 11 APR 2017
Accepted article online 14 APR 2017
Published online 3 MAY 2017

Modes of temperature and pressure variability in midlatitude troposphere and lower stratosphere in relation to cosmic ray variations

A. L. Morozova[1], J. J. Blanco[2], and P. Ribeiro[1,3]

[1]CITEUC, University of Coimbra, Coimbra, Portugal, [2]Department of Physics and Mathematics, University of Alcalá, Madrid, Spain, [3]Geophysical and Astronomical Observatory, University of Coimbra, Coimbra, Portugal

Abstract The study is based on the analysis of atmospheric and space weather parameters in the midlatitude region (Iberian Peninsula) during, approximately, the epoch of the 24th solar cycle maximum. The principal component analysis was applied to sets of air temperature and geopotential height measurement at different pressure levels from a near-ground level (930 hPa) to the stratosphere (up to 10 hPa). The analysis of extracted modes shows couplings between atmospheric and medium-term variations (from weeks to months) of space weather parameters. The first mode of the atmospheric variability is related to the atmospheric dynamic processes that are common for the extratropical Northern Hemisphere. Extracted temperature and pressure variations are located in the upper troposphere-lower stratosphere region and positively correlate with ozone content variations. Among space weather parameters, this atmospheric mode shows statistically significant negative correlation with the ground-measured cosmic ray flux measured by the Castilla-La Mancha neutron monitor (Spain) and weaker or no correlation with geomagnetic parameters.

Plain Language Summary The study is based on the analysis of the conditions in the troposphere and stratosphere above the Iberian Peninsula. Mathematical methods were applied to the data to extract different modes of atmospheric variability that are coupled with changes of geophysical parameters. In this paper the variations of the temperature and pressure coupled to the cosmic ray flux are considered. The possible mechanisms are discussed.

1. Introduction

Earth's environment is strongly affected by external forcings. The atmosphere is continuously bombarded by primary cosmic rays (CRs) of different energies. Solar wind, both fast and slow streams, and embedded magnetic structures such as shock waves, interplanetary coronal mass ejections, or magnetic clouds transported by them interact in a very effective way with the Earth's magnetosphere and affect thermosphere density and temperature [see, e.g., *Guo et al*., 2010; *Knipp et al*., 2013; *Mlynczak et al*., 2015]. Long- and short-term variations of solar activity disturb the Earth's magnetosphere resulting in geomagnetic storms, radio blackouts, auroras, and other events. Deeper in the Earth's atmosphere at different altitudes, injected particles interact with the Earth's magnetic and electric fields and with molecules and atoms of air causing many geophysical phenomena (e.g., air ionization, production/destruction of molecules of small air constituents like ozone and NO_x, variations of the low atmosphere electric field, and ionospheric disturbances). Some of these events are studied very well using both data analysis and theoretical modeling; others, related, in particular, to effects of the energetic particles on atmospheric conditions, are subjects of ongoing discussions (see, e.g., reviews by *Danilov and Laštovička* [2001], *Haigh* [2003], *Krivolutsky* [2003], *Baldwin et al*. [2007], *Carslaw* [2009], *Mironova et al*. [2015], and *Yiğit et al*. [2016]).

The primary and secondary particles of the CR are the main ionizing source in the atmosphere between ~5 km and ~60 km above the ground [*Bazilevskaya*, 2000]. Solar activity modulates the low-energy and most abundant component (from hundreds of MeV to tens of GeV) of the galactic CR flux at the top of the Earth's atmosphere, both on the long (e.g., 11 year solar cycle) and short time scales (e.g., Forbush decreases or recurrent disturbances with 27 day period). Forbush decreases (FDs) were first defined by S. E. Forbush in the 1930s as a decrease in the CR flux [*Forbush*, 1938]. They can last from hours to several days and have amplitudes of up to ~20% of the nondisturbed previous CR flux. The strength (depth) of an FD depends not only on the

solar wind conditions but also on geomagnetic latitude since the probability for a charged particle to penetrate the Earth's atmosphere depends on both the particle's energy and the geomagnetic shielding effect. The parameter commonly used to describe this shielding effect by both the geometry and intensity of the geomagnetic field (GMF) is the geomagnetic cutoff rigidity R_c [*Dorman*, 2009]. The ground-based CR detectors measure, as a rule, not primary CR particles but those generated in the so-called atmospheric showers—processes of generation of the secondary particles in collisions of the energetic particles with atmospheric atoms and molecules [*Nakamura*, 2010]. Most of the ground-based low-energy CR detectors are designed to measure neutrons (neutron monitors) or muons (muon telescopes) [*Clem and Dorman*, 2000; *Nakamura*, 2010].

Interaction between the CR particles and the low atmosphere (troposphere and the lower stratosphere) is complex. The intensity of the ground-measured secondary particles depends on the atmospheric depth—an integral in altitude of the atmospheric density above a specific level [*Bazilevskaya*, 2000; *Clem and Dorman*, 2000]. The most important parameters for the ground-measured CR flux are pressure (in case of muons and neutrons) and temperature (in case of muons) at altitudes between 11 and 16 km (top troposphere-tropopause region in midlatitudes) where the majority of secondary particles are produced [*Aplin et al*., 2005]. The standard corrections procedure for the ground-based CR detectors is traditionally based on the pressure and temperature in the detector surrounding area [e.g., *Clem and Dorman*, 2000] and on the assumption of the standard atmosphere model [*Atmosphere, U.S*., 1976]. The analysis of the ground-measured CR flux shows that this procedure performs very well in the case of neutron monitors and relatively well in the case of muon telescopes [*Clem and Dorman*, 2000; *Dorman*, 2009]. This difference between the neutron and muon flux variations is due to the physics of the process of secondary particles production and their further interactions with atmospheric atoms and molecules. As a result, a dependence of the ground pressure-corrected muon telescope data with the conditions in the top troposphere-stratosphere is observed [see, e.g., *Osprey et al*., 2009; *Braga et al*., 2013]. On the other side, the "atmospheric effect" on the ground-measured neutron flux was considered completely removed by the corrections to the ground-measured atmospheric pressure. However, in recent years a number of studies [*Aplin et al*., 2005; *Sloan et al*., 2011; *Harrison et al*., 2014] showed relations between neutron monitor measurements (primary particles with energies of about 10^0–10^1 GeV) and thermodynamic conditions of the atmosphere at ~100–30 hPa (tropopause or lower stratosphere regions, depending on the latitude). The amplitude of the reported atmospheric effect is ~1% averaged over the globe [*Aplin et al*., 2005] and falls in the same range as the previously found effect of the CR particles on Earth's weather and climate [see *Carslaw*, 2009; *Lockwood*, 2012, and references therein] that is believed to be related to changes produced by the charged particles in the chemical composition and dynamics of the lower stratosphere and troposphere [*Haigh*, 2003; *Baldwin et al*., 2007; *Bazilevskaya et al*., 2008]. Therefore, further studies are needed to disentangle the problem of mutual impacts of atmospheric conditions and CR flux.

Another space weather parameter that is believed to influence the lower atmosphere conditions is the GMF and its main short-term variations—geomagnetic storms [see, e.g., *Le Mouël et al*., 2009, and references therein]. Although the geomagnetic storms and FD are caused by different physical mechanisms, they are often observed together. However, the relation between the variations of the GMF and CR flux is not straightforward. For example, significant FDs are seen during both the magnetically disturbed and quiet days [*Kudela and Brenkus*, 2004]. Contrary to the CR case, the mechanisms that can explain covariations of the atmospheric and geomagnetic parameters are controversial. Among the more reliable hypotheses we can mention variations of the electric atmospheric field (see review in *Tinsley* [2008] and *Tonev and Velinov* [2015]) and/or solar irradiance in UV and X-ray part of the spectrum [e.g., *Haigh*, 2003].

Most of the studies searching for the coupling between space weather and the lower atmosphere are based on the analysis of conditions in the high latitudinal or equatorial regions and consider midlatitudinal atmosphere to be affected by the space weather in a weaker or even negligible way. Nevertheless, interest in the mid-latitudes has increased over the last few years resulting in several papers analyzing relations between the atmospheric conditions in this region and different space weather parameters [e.g., *Goncharenko and Zhang*, 2008; *Pancheva and Mukhtarov*, 2011]. The relative lack of interest in the middle latitudes is related to the fact that the midlatitude regions (due to the GMF configuration) are not strongly affected by the intense fluxes of the energetic particles from the CR, solar wind, and different magnetospheric regions. The auroral substorms are not usually observed in midlatitudes, and the amplitude of geomagnetic

storms is much lower than at higher latitudes. Strong ionospheric disturbances frequently seen in the equatorial region rarely extend to the middle latitudes. However, FD, geomagnetic storms, and ionospheric disturbances [e.g., *Laštovička*, 1996; *Danilov and Laštovička*, 2001; *Tsagouri et al*., 2000; *Maruyama and Nakamura*, 2007] do exist in midlatitudinal regions and can affect middle and low atmosphere directly. Moreover, the circulation patterns in the Northern Hemisphere are controlled by the quasi-biennial oscillations (QBO) of the direction of the stratospheric zonal winds near the equator and the polar vortex (PV) conditions. An increase of the meridional circulation can result in an intense exchange of air masses between the space weather-affected polar/equatorial regions and middle latitudes. Thus, the temperature and composition of the midlatitudinal troposphere and stratosphere can be indirectly affected by space weather events.

As one can see, the relationship between the solar activity, CR flux, magnetosphere, and atmosphere is very complex. Nevertheless, local/regional studies can be a suitable approach to shed some light on processes responsible for covariability between space weather and atmospheric parameters [*Lockwood*, 2012]. In this paper, we present an analysis of the coupled variations of the locally measured atmospheric parameters like temperature and pressure in the troposphere, tropopause, and lower stratosphere over a midlatitudinal region (Iberian Peninsula) and variations of the space weather and space weather-driven parameters like the stratospheric ozone content (O_3), locally measured CR flux, GMF horizontal component, and the solar UV flux. The analyzed data cover a 2 year period from 1 July 2012 to 30 June 2014 allowing us to compare relations between the atmospheric and space weather parameters under both the east and west phases of QBO.

The paper is organized as follows: section 2 contains the descriptions of the analyzed data sets and section 3 describes the applied mathematical methods. In section 4, a short review of the atmospheric and space weather conditions during the studied period is given. Results of the analyses are presented and discussed in section 5. Finally, section 6 shows a summary and the main conclusions.

2. Data

2.1. Atmospheric Data

2.1.1. Madrid Sounding Series

Altitudinal profiles of meteorological parameters used in this study are part of the Integrated Global Radiosonde Archive database that collects data from over 1500 globally distributed stations of radiosonde and balloon observations. Bidaily (00:00 and 12:00 UTC) observations are available for different altitude levels (between 930 and 30 hPa) and include, among other parameters, pressure, temperature, and geopotential height. In this study, we used data from the sounding station at Madrid airport (08221, LEMD, 40.50°N, 3.58°W, 633 m above sea level (asl)) from 1 July 2012 00:00 to 30 June 2014 12:00. This data set has few gaps: 73 missed/failed observations (5% of all data) and 17 incomplete observations (~1%) with valid data only from the ground up to heights ranging between 300 and 100 hPa. The selected parameters for this study are the altitude (*h*, in m), atmospheric pressure (*p*, in hPa), and air temperature (in °C). Since each of the observations has its own specific height-pressure scale, all the observations were rescaled (using the linear interpolation) into pressure intervals of 10 hPa (91 levels). The pressure scale was chosen considering both the predominant weather conditions in the studied region and the availability of the measurements at high-altitude levels as well as the intervals between the pressure levels: 10–30 hPa near the ground and in the middle troposphere and a couple of hPa in the upper part of the balloon's flight. Consequently, the analysis was done for two meteorological parameters: the geopotential height of a specific pressure level (*gph*) and the air temperature at this level (*T*). The time variations of the original *T* and *gph* altitudinal profiles are shown in Figures 1a and 1d, respectively, and the monthly averaged height profiles are in Figures 1b and 1e.

2.1.2. Stratospheric Parameters

Variations of the stratospheric temperature at different pressure levels were analyzed using the data for the zonally averaged temperature at 50°N (T_{50N}) and 80°N (T_{80N}) at different stratospheric pressure levels (from 150 to 10 hPa) available from 1979 to the present from the Modern-Era Retrospective Analysis for Research and Applications (MERRA) database. Another data set containing the information on the stratospheric temperature variations used in this study is the Aqua Atmospheric Infrared Sounder (AIRS) Level 3 Daily Standard Physical Retrieval (AIRS + AMSU (advanced microwave sounding unit)), AIRX3STD. We used area averaged data of the temperature at 50 hPa and 10 hPa levels over the whole Iberian Peninsula (from

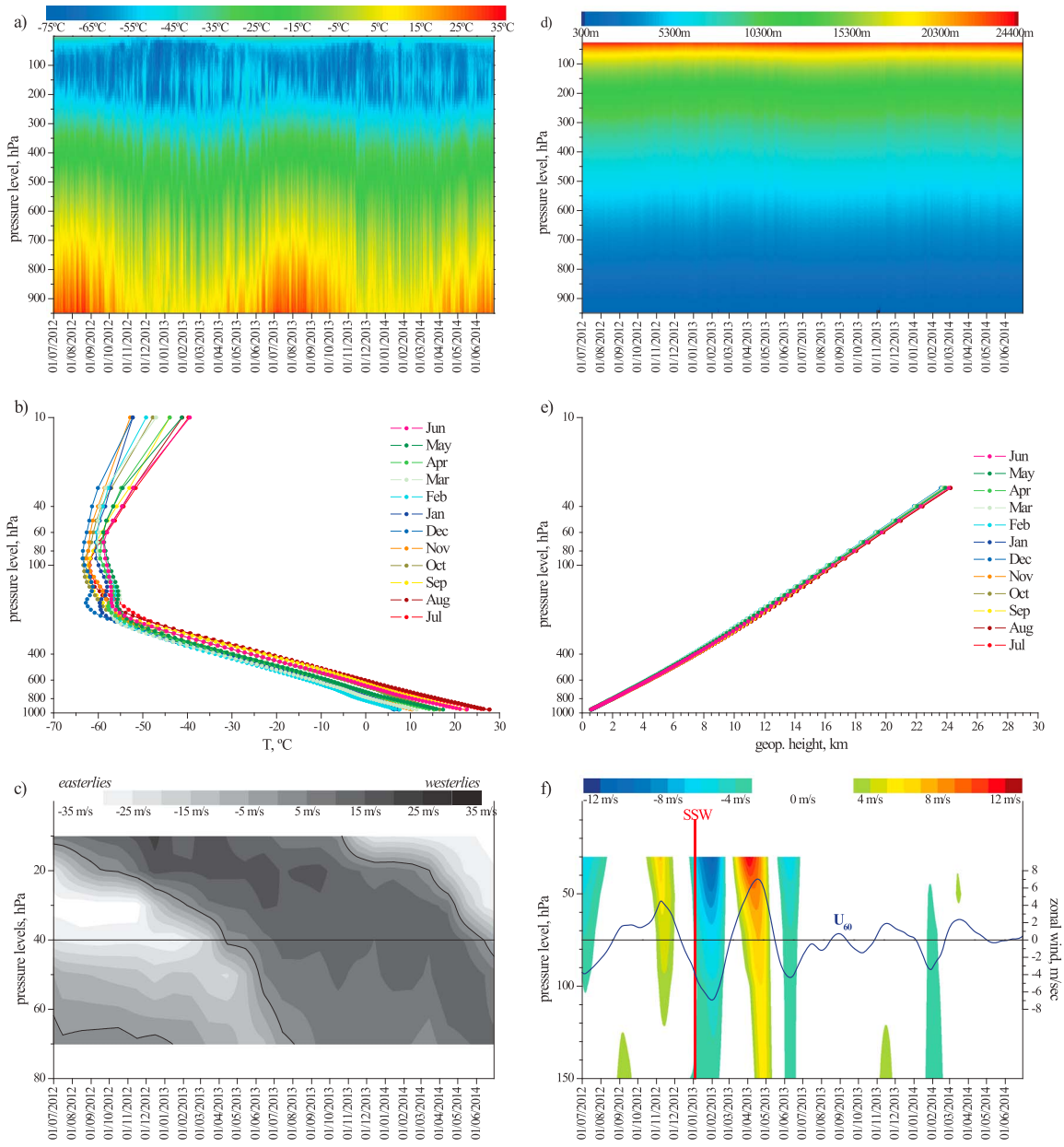

Figure 1. Altitudinal profiles of the (a and b) atmospheric temperature and (d and e) geopotential height from 1 July 2012 00:00 to 30 June 2014 12:00: original rescaled and interpolated bidaily data (Figures 1a and 1c) and monthly averaged altitudinal profiles (Figures 1b and 1e). (c) Velocity and direction of the equatorial stratospheric QBO winds (westerlies are positive). (f) Variations of the stratospheric zonal wind U at 60°N from the annual cycle (westerlies are positive) at different pressure levels (color map) and their average (line); vertical red line marks the SSW event.

350°W to 0°W in longitude and from 36°N to 44°N in latitude). The Iberian Peninsula temperature series correlate with the corresponding Madrid sounding temperature data at the 50 hPa level very well. Therefore, the Iberian Peninsula area averaged and the Madrid balloon data sets were combined to increase the range of the altitude used in this work (from 930 hPa to 10 hPa) and to include atmospheric levels that play a central role in the first interaction between primary cosmic rays and atmospheric molecules.

Since the dynamics of the stratosphere is strongly affected by the QBO, its phases were defined using the data of the monthly mean equatorial zonal wind components at different stratospheric pressure levels (from 70 to 10 hPa) available from 1953 to the present in the Freie Universität Berlin database. They are shown (for the studied period) in Figure 1c (white shades for easterlies, eQBO, and black shades for westerlies, wQBO). The dynamics of the stratosphere in middle and high latitudes of the Northern Hemisphere is described by

the zonal mean stratospheric zonal wind (*U*) at 60°N for 150–30 hPa pressure level MERRA reanalysis database (Figure 1f).

To analyze the stratospheric ozone variations, we used the area-averaged (over the Iberian Peninsula) measurements of both the ozone total column values ($O_{3\ tc}$, in DU) and the ozone mole fraction in air measured at the 50 hPa and 10 hPa levels ($O_{3\ 50}$ and $O_{3\ 10}$, correspondingly). These data sets are from AIRX3STD v006 data set.

2.2. Solar and Space Weather Data

2.2.1. Cosmic Rays

Neutron monitors are very good instruments to monitor CR and solar energetic particles (SEPs) with energy of about a few GeV because of their stability in long- and short-term observations. The energy detection threshold in a neutron monitor depends on its rigidity cutoff. Although the global picture observed by neutron monitors is similar, slight differences exist depending on their geographical location and rigidity giving a "local" picture of the CR coming to a specific station. This is clearly observed during short-term variations caused by solar activity as, for instance, ground level enhancements and FD. Examples of such "nonsimultaneous" FD are presented in *Oh et al*. [2008]. The CR flux variations analyzed in this study are from the ground *Castilla-La Mancha Neutron Monitor*, *CaLMa* (Guadalajara, Spain, 40.63°N, 3.15°W, 708 m asl) [*Medina et al*., 2013]. This station, with a vertical cutoff rigidity R_c = 6.95 GV, gives a direct measurement of the CR arriving to the Iberian Peninsula. Please note that most of the incoming CR arrive from directions quite apart from the vertical. Real-time measurements are uploaded to the Neutron Monitor Database (NMDB) with a 1 min cadence. In our analysis we used pressure- and efficiency-corrected data. The comparison to data obtained by other neutron monitors shows that the series obtained by CaLMa are in good agreement both with data from monitors with similar R_c (Rome, R_c = 6.27) and with data from monitors with lower geomagnetic cutoff rigidity (Apatity, R_c = 0.65 or Oulu, R_c = 0.81). This agreement exists on both the long and short time scales. CaLMa data (hereinafter *CR*) are available from 11 July 2012, 12:00 and contain only 1 day long gap from 7 January 2014, 09:36:00 to 8 January 2014, 10:29:00 caused by a temporal malfunction in CaLMa power supply.

2.2.2. Geomagnetic Field

To analyze the geomagnetic field variations, two parameters were used. The first one is the global *Dst* ("disturbance storm time") index. Its hourly values are derived from a network of near-equatorial ground observatories to monitor the geomagnetic horizontal component disturbances associated to the axially symmetric magnetic variations produced by magnetosphere currents. Major events in *Dst* variations, corresponding to a negative variation, are produced mainly by the equatorial current system in the magnetosphere (ring current), while minor positive deviations are mostly caused by the compression of the magnetosphere from solar wind pressure increases [*Sugiura and Kamei*, 1991].

Another parameter (hereinafter, *COI H*) characterizing local geomagnetic field variations is based on the measurements of the horizontal component of the GMF at the *Coimbra Magnetic Observatory* (IAGA code COI, Coimbra, Portugal, 40.22°N, 8.42°W, 99 m asl). The COI station, operated by the *Geophysical and Astronomical Observatory* of the University of Coimbra (GAOUC), is equipped with a triaxial fluxgate magnetometer (FGE model with a tilt-compensating suspension) for the continuous recording of magnetic variations of horizontal, declination, and vertical (*H*, *D*, and *Z*) components. During the studied period there were 37 minor gaps in the *COI H* bidaily data series (2.3% of the data length); the two bigger gaps occurred between 19 January 2013 and 28 January 2013 and between 26 March 2014 and 1 April 2014. The *COI H* hourly data can be considered (after the removal of the secular trend) as a local version of the *Dst* index. In this study we did not analyze other geomagnetic field components affected by the solar activity variations (e.g., *D* and *I* components) because they are strongly correlated with the *COI H*.

Since the distance between the stations measuring the *COI H*, *CR*, and atmospheric parameters (Madrid sounding series) does not exceed ~400 km, in the frame of this study, all these parameters can be considered as "locally measured."

2.2.3. Remote Solar and In Situ Solar Wind Observations

Solar activity and solar wind conditions have been analyzed to provide the needed Sun-Earth interaction context. Solar activity level was evaluated using the coronal mass ejection (CME) observations from the Large Angle and Spectrometric Coronagraph on board SOHO spacecraft and the number of X-class flares observed by the GOES satellites. Solar wind conditions around the Earth were evaluated using the

interplanetary magnetic field, solar wind velocity, density, and temperature measured by different spacecraft which were provided by the OMNI database and the SOHO Electron Proton Helium Instrument (EPHIN). These data were used to identify structures and specific conditions in the solar wind at the Earth's orbit (see Table S1 in the supporting information).

Variations of the solar UV radiation were parameterized using the Mg II composite series [*Snow et al*., 2014] based on the measurements of the emission core of the Mg II doublet (280 nm). It is frequently used as a proxy for solar irradiance variability in the spectral range from UV to EUV [*Hood*, 2004; *Snow et al*., 2014] and shows strong variability due to the 11 year solar cycle and solar rotation (~27 days).

3. Methods

3.1. Data Preprocessing

All data series (except *CR* series) used in this analysis start on 1 July 2012 and end on 30 June 2014 and are of daily or, when possible, bidaily (00:00 and 12:00 UTC) time resolution. The data preprocessing consisted in gaps interpolation and rescaling to the uniform pressure scale of the altitudinal profiles of the atmospheric parameters. Since the data set covers two consecutive years, the annual cycles (*AC* series) have to be removed from most of the analyzed parameters (namely, all temperature series, *gph*, *U*, and all ozone series). The series of *COI H* and Mg II contain significant variations related to solar activity variations and, in case of *COI H*, to the trends of the internal component of the GMF. These variations were also named "*AC* series" for simplification. Procedures used to extract the *AC* series are described in section 3.3.

3.2. Principal Component Analysis

The principal component analysis (PCA) is a well-known method to extract independent spatial-temporal modes of variability (principal components, PCs, for time series and empirical orthogonal functions, EOFs, for spatial patterns) when a number of series of the same parameter from different stations (grid points, altitude levels, etc.) is used. This method is based on the calculation of the eigenvalues and eigenvectors of the covariance matrix constructed from the input data set. It also estimates the "weights" (or explained variances, *f*) of the extracted modes. The PCs are orthogonal and conventionally nondimensional. The full descriptions of the method can be found in, e.g., *Bjornsson and Venegas* [1997], *Hannachi et al*. [2007], and *Shlens* [2009]. In some cases the rotation of the eigenvector matrix is proved useful. Here we used the varimax and dual varimax rotation methods [*Bjornsson and Venegas*, 1997].

Since we analyzed two coupled meteorological variables (*T* and *gph*), an extension of the PCA, a singular value decomposition of the coupled fields (hereafter "cSVD"), was used to study time-space variability patterns common to both the *T* and *gph* series. This method differs from the standard PCA in the way of construction of covariance (or correlation in our case) matrix. The description can be found in *Bjornsson and Venegas* [1997] and *Hannachi et al*. [2007]. The cSVD analysis extracts the modes of variability that are common for both of the series. In our case, the temporal and spatial patterns extracted by the PCA and cSVD analyses for each of the atmospheric parameters are very similar but the values of explained variance are different.

Some of the variability modes of the *T* and *gph* series show statistically significant correlations with space weather parameters (described in section 2.2) and ozone content. In this paper we focus only on the first mode: PC1/EOF1 both from the PCA and cSVD. The second and the third modes that show covariability with geomagnetic and ionospheric parameters will be discussed in a future paper.

The PCA was also used to calculate the mean variations of atmospheric parameters measured at different altitudes (PC1 for the *U*, T_{50N}, and T_{80N} series).

3.3. Decomposition

To extract the *AC* series from the analyzed data, the PCA was applied to the original series with small modifications depending on the length of the available data sets (please also see the supporting information for the *AC* series plots and discussion).

For the parameters that are available for at least a 10 year time interval (*U*, stratospheric temperatures, and ozone), the *AC* series were obtained from the original ones using only the PCA (PC1s).

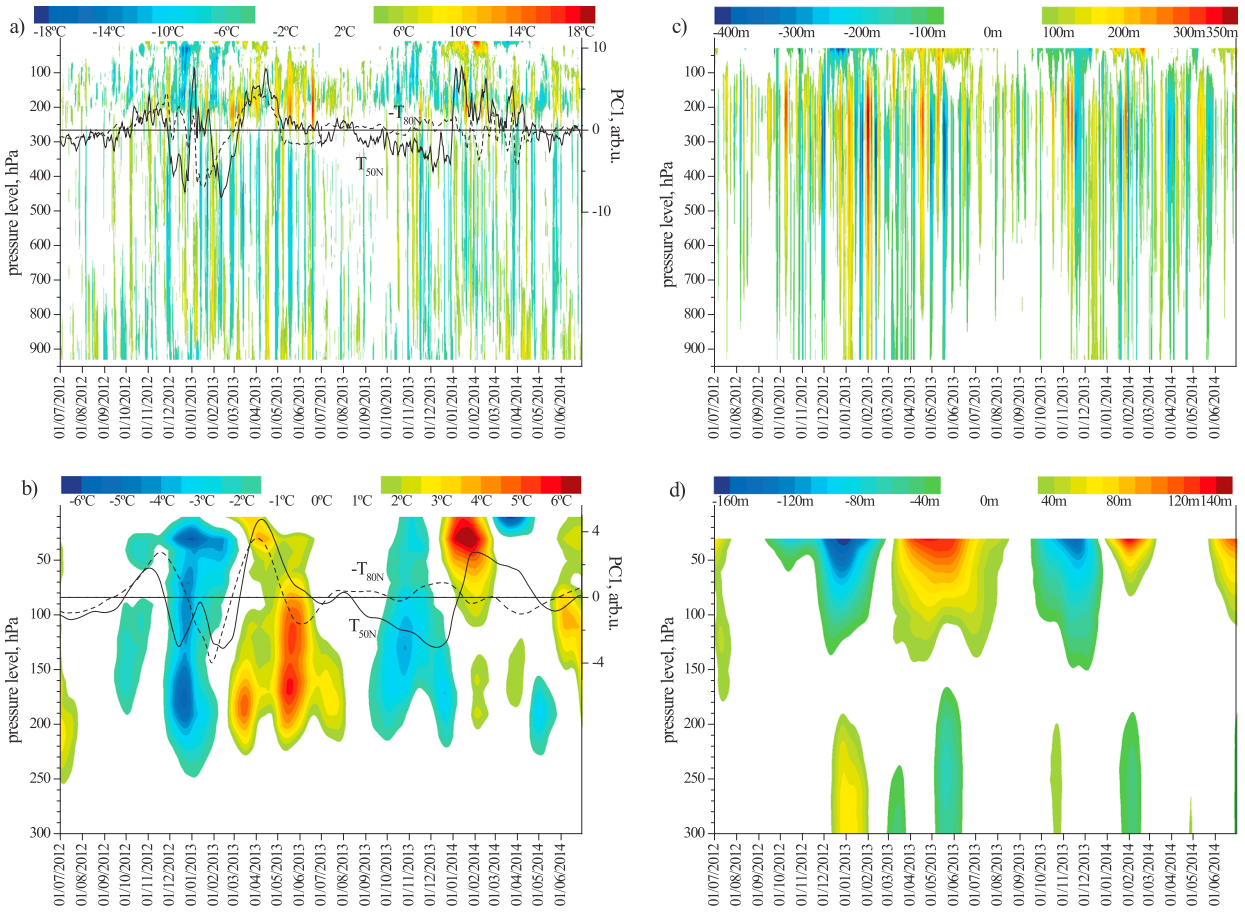

Figure 2. Variations of the (a and b) temperature and (c and d) *gph* altitudinal profiles (colors): *noAC* (Figures 2a and 2c) and *Smoothed* (Figures 2b and 2d) series. Stratospheric temperatures T_{50N} (solid lines) and T_{80N} (dashed lines, reversed sign): PC1 (Figure 2a) and *Smoothed* PC1 (Figure 2b). Please note different color scales for the *noAC* and *Smoothed* series.

The series of the atmospheric sounding parameters (*T* and *gph*) have a limited time length (2 years) and therefore have to be smoothed before the PCA to ensure that variations due to the year-to-year weather changes are not filtered to the *AC* series. The original series were first submitted to a decomposition procedure named a seasonal-trend decomposition based on LOESS or STL (see *Cleveland* [1979], *Cleveland and Devlin* [1988], and *Cleveland et al.* [1990] for details; this procedure is also shortly described in *Morozova and Barlyaeva* [2016]). Then the smooth STL trend components of the *T* and *gph* series were submitted to the PCA. The resulting PC1s were considered as the *T* and *gph* annual cycles (shown in the supporting information).

Since the series of *COI H* and Mg II show no significant annual variations, the extraction of their *AC* series was based only on the STL decomposition procedure.

All above mentioned parameters were submitted for further analysis in the form of variations relatively to their *AC* series (hereafter, *noAC* series). Series of the *CR* and *Dst* show no visible annual or other trends during the studied period.

The preliminary analysis of the *noAC* series shows existence of both long-term (with a characteristic period of weeks to months) and short-term (with a period of a couple of days) variations. In this paper we analyze only the variability on the long-term time scale (as just defined). To extract this kind of variations (*Smoothed* series), we applied the STL decomposition to all the *noAC* series and to the *CR* and *Dst* original series. Figures 2b and 2d show altitudinal profiles of the *Smoothed* components of the *T* and *gph* series, respectively, Figure 1f shows the *Smoothed noAC* series of *U* (at different pressure levels and the average), Figures 2a and 2b show also the *noAC* and *Smoothed* series of the PC1 of T_{50N} and T_{80N}, and Figure 3

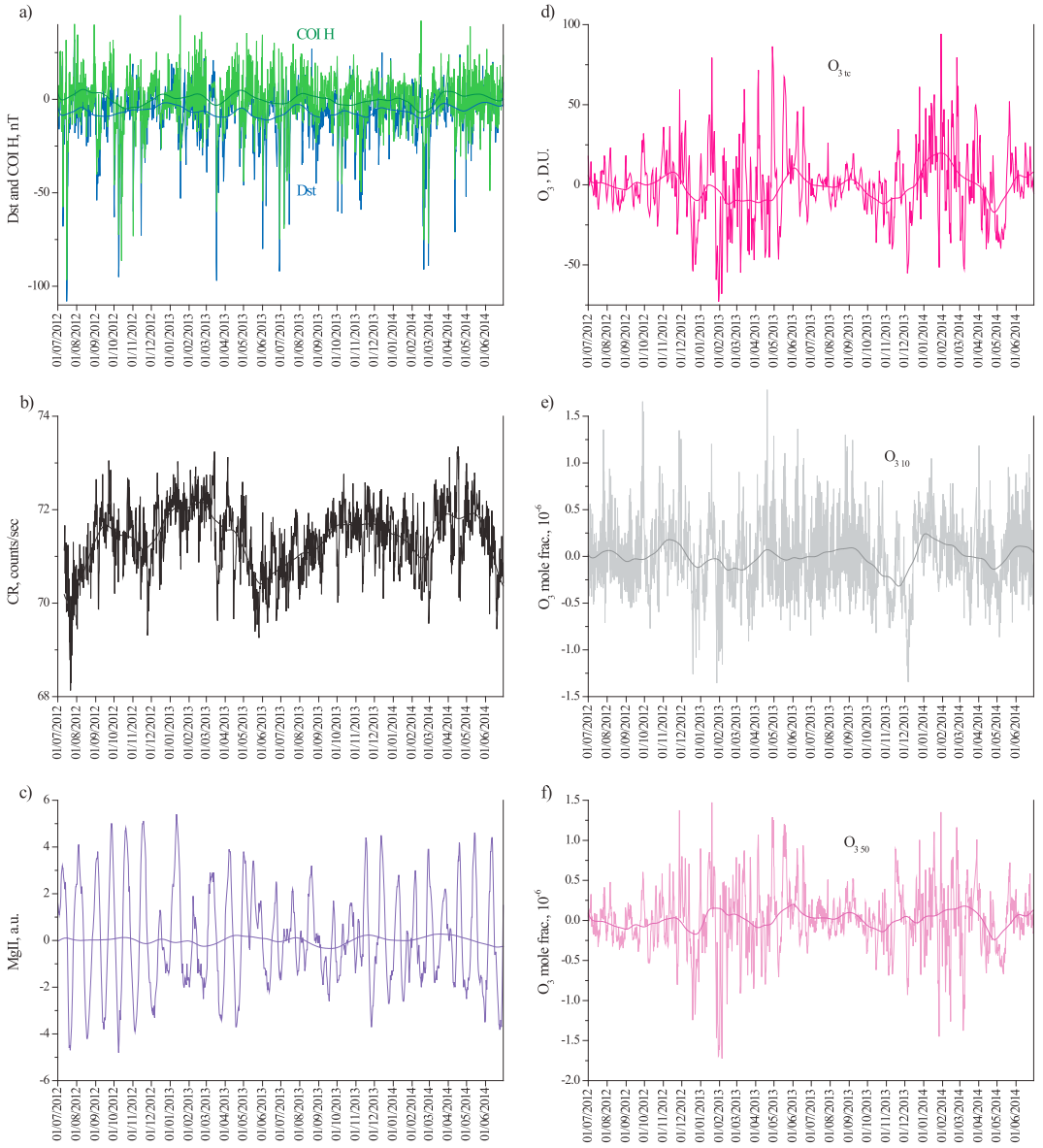

Figure 3. (a) Original/*noAC* (thin line) and *Smoothed* (thick line) series of *Dst* (blue)/*COI H* (green). (b) Original (thin line) and *Smoothed* (thick line) series of CR. (c) *noAC* (thin lines) and *Smoothed* (thick lines) series of Mg II. (d–f) *noAC* (thin lines) and *Smoothed* (thick lines) series of the ozone series: $O_{3\ tc}$ (Figure 3d), $O_{3\ 10}$ (Figure 3e), and $O_{3\ 50}$ (Figure 3f).

shows the *noAC* (original for *CR* and *Dst*) and *Smoothed* components of the space weather parameters and the ozone series. Overall, the data smoothed using this procedure are similar to those obtained with a moving averaging procedure (in our case, with windows of approximately 1.5–2 weeks long). Please note that the amplitude of the *Smoothed CR* series is about 2 c/s or ~3% of the mean CR flux measured during the studied period by the CaLMa.

3.4. Correlation Analysis

The similarities between the variations of the atmospheric and geophysical parameters were studied using the correlation analysis. The correlation coefficients (*r*) were calculated between the series of the space weather and atmospheric parameters used in this study, as well as between PCs (both from PCA and cSVD) of the *T* and *gph* series and the series of the space weather parameters. To avoid uncertainty that could arise from the smoothing procedure (STL), the correlation coefficients for the *Smoothed* series were calculated for the period from 1 August 2012 to 31 May 2014.

Table 1. Correlation Coefficients Between the Space Weather Parameters (Including Ozone)[a]

	CR	*Dst*	*COI H*	Mg II	$O_{3\ 10}$	$O_{3\ 50}$	$O_{3\ tc}$
(A) AC Series \ Original Series							
CR					-0.32 (<0.01)		
Dst	x		0.53 (<0.01)				
COI H	x	x		0.24		0.28	0.48
Mg II	x	x	0.63			0.2	0.2
$O_{3\ 10}$	x	x	0.21				0.37 (<0.01)
$O_{3\ 50}$	x	x	0.38	0.42	−0.42		0.8 (<0.01)
$O_{3\ tc}$	x	x	0.58 (0.01)	0.26	0.34	0.67 (0.09)	
(B) Smoothed Series \ noAC Series							
CR							
Dst	0.37 (0.07)		0.75 (<0.01)				
COI H		0.45 (0.01)					
Mg II							
$O_{3\ 10}$	−0.44 (0.04)					0.46 (<0.01)	0.87 (<0.01)
$O_{3\ 50}$	−0.29	−0.25	−0.23		0.31 (0.11)		0.55 (<0.01)
$O_{3\ tc}$	−0.51 (0.02)		−0.37		0.76 (<0.01)	0.61 (<0.01)	

[a]Values above diagonals are for the original (A) and *noAC* (B) series. Values below diagonals are for the *AC* (A) and *Smoothed* series (B). There are no *AC* series for CR and *Dst* ("x" marks). Only correlation coefficients $|r| \geq 0.2$ are shown; p values ≤ 0.1 are in brackets.

The significance of the correlation coefficients was estimated based on a nonparametric Monte Carlo approach using artificial series. These series were constructed by two different methods. For the original and *noAC series* we utilized the "phase randomization procedure," consisting in the direct fast Fourier transform (FFT) followed by the inverse FFT with the same power spectrum but random phase [*Ebisuzaki*, 1997]. For the *AC* and *Smoothed* series the "bootstrapping with moving blocks" randomization procedure [*Künsch*, 1989; *Lahiri*, 1999] was used. The randomization procedures create an artificial series with the same autocorrelation as the original one. The artificial series are then subjected to the same type of correlation analysis as the original ones. The obtained statistical significance (p value) takes into account the probability of a random series to have the same (or higher) absolute value of r as in case of a specific pair of the original series.

The correlation coefficients between the series of the space weather parameters used in this study are shown in Table 1 for the original, *AC*, *noAC*, and *Smoothed* series. Table 2 contains correlation coefficients for the *Smoothed* PC1s of the *T* and *gph* series and the *Smoothed* series of the space weather parameters.

Table 2. Parameters of PC1s of the *Smoothed T* and *gph* Series (PCA—Explained Variance Fraction *f* and cSVD—Analogue of *f* and the Squared Covariance Fraction f_2) and Correlation Coefficients Between PC1s and the *Smoothed* Series of Space Weather Parameters[a]

		r (*p* Value)						
	f or *f* (f_2) (%)	*CR*	*Dst*	*COI H*	Mg II	$O_{3\ 10}$	$O_{3\ 50}$	$O_{3\ tc}$
T								
PCA	66.7	−0.45 (0.05)	−0.29			0.31	0.51 (<0.01)	0.31
cSVD	79.0 (98.0)	−0.47 (0.04)	−0.32 (0.1)			0.33	0.51 (0.06)	0.33
gph								
PCA	77.0	−0.5 (0.02)	−0.44 (0.02)		−0.21	0.39 (0.06)	0.37 (0.05)	0.35 (0.1)
cSVD	79.0 (98.0)	−0.51 (0.02)	−0.43 (0.03)		−0.2	0.4 (0.06)	0.39 (0.04)	0.36 (0.1)

[a]Only correlation coefficients $|r| \geq 0.2$ are shown; p values ≤ 0.1 are in brackets.

4. Review of Atmospheric and Space Weather Conditions During the Studied Period

4.1. Atmosphere

The Madrid area (as well as most part of the Iberian Peninsula) is a region with a Mediterranean climate with continental influence [*Andrade and Corte-Real*, 2016] which is characterized by mild cold winters and hot summers [*De Castro et al*., 2005]. During the studied period, temperature and pressure fields show variations related both to the regional climatic features and to the hemispheric atmospheric circulation. The monthly mean altitudinal profiles of the original *T* and *gph* series shown in Figures 1b and 1e, correspondingly, show a tropopause located between ~200–150 hPa and ~50 hPa (between 12 and 20 km). The annual temperature and pressure cycles in the troposphere below ~900 hPa agree with previous observations [see, e.g., *De Castro et al*., 2005], and in the free atmosphere the onsets of the annual temperature minima and maxima slightly change with altitude.

The variations of the *Smoothed* components of the temperature and *gph* altitudinal profiles (Figures 2b and 2d, correspondingly) have maximal amplitudes in the atmosphere above ~300 hPa—free troposphere, tropopause, and lower stratosphere. The amplitudes of the *T* and *gph* variations below ~300 hPa are more than 2 times lower. The comparison of the *Smoothed* components of the *T* and *gph* series shows that their variations are in phase from the ground to ~300 hPa (~10 km) level.

The variations of the temperature in the upper troposphere-lower stratosphere region display features similar to ones observed in stratosphere by other instruments (see section 2.1.2) The periods of stratospheric cooling and warming are clearly seen in the Madrid sounding and satellite data (Figures 2a and 2b). These periods are in close agreement with variations of the zonally averaged stratospheric temperature T_{50N}. We applied PCA to the series of T_{50N} at different altitudes and compared the obtained PC1 (shown in Figure 2a as a solid line) to the sounding *T* profiles. For some periods the variations of the stratospheric temperature above the IP were found lagged behind T_{50N} in a range between 1 and 2 weeks.

The analysis of the stratospheric data allowed us to mark autumn 2012, winter 2012–2013, and autumn 2013 as periods of colder than normal stratosphere, whereas winter-spring 2013, summer 2013, and winter-spring 2014 can be identified as periods of warmer than normal stratosphere and upper troposphere (Figures 2a and 2b). A strong Sudden Stratospheric Warming (SSW) event took place in the beginning of January 2013 significantly affecting the NH atmosphere in the later winter-spring and even summer of 2013 [*Coy and Pawson*, 2015]. SSW events are characterized by the sudden and fast warmings of the polar stratosphere as is seen in the T_{80N} variations (Figure 2a, black dashed line plotted with reversed sign) and by the change of the strength and direction of the zonal wind *U* (Figure 1f). The winter 2013–2014 was characterized by the strong PV leading to a colder polar and warmer midlatitudinal stratosphere [*Ern et al*., 2016]. The variations of the stratospheric temperature in the polar region (T_{80N}) anticorrelate with the ones in middle latitudes (T_{50N} and *T*). As one can see, the onset of the SSW in the polar regions results in a cooling of the midlatitudinal stratosphere (as was discussed earlier in *Limpasuvan et al*. [2004, 2005]).

The first half of the analyzed time period (before approximately June 2013) was characterized by the easterly winds in the equatorial atmosphere at 60–70 hPa level (eQBO), whereas during the second half (from approximately July 2013) they were replaced by the westerlies (wQBO)—Figure 1c. Since the QBOs affect meridional circulation over the whole Northern Hemisphere and polar stratospheric conditions [*Lu et al*., 2008], we could find differences (if any exist) in relations between the atmospheric (e.g., ozone) and space weather parameters that are QBO dependent.

Ozone abundance is an atmospheric parameter closely linked to solar activity. At the same time, as atmospheric parameter, it is directly related to the QBO [*Balachandran and Rind*, 1995]. The ozone series variations show significant annual cycle (see supporting information) with slightly shifted dates of the minima/maxima for different parameters. The variations of the temperatures above the 150 hPa pressure level (a region where amplitude of temperature variations is maximal) show statistically significant correlation with the ozone variables. The $O_{3\ tc}$ and $O_{3\ 10}$ *noAC* series correlate with atmospheric temperature series at 50 hPa pressure level: $r = 0.53$–0.76 (p values ≤ 0.07). On the other hand, the $O_{3\ 50}$ *noAC* series shows dependence on *U* ($r = -0.33$ to -0.37, p value = 0.05–0.09), *T* at 150 hPa ($r = 0.53$, p value < 0.01), and *gph* at 200 hPa level ($r = -0.63$, p value < 0.01).

4.2. Space Weather

During the studied period mild space weather conditions were observed. Overall, 4843 CME were recorded among which 147 (3%) were of halo type. However, there were 23 geomagnetic storms ($Dst \leq -50$ nT) and only eight of them can be classified as strong with $Dst \leq -100$ nT (see a list of events in the supporting information). The relatively low number of great storms during the studied period, which coincides with the 24th solar cycle maximum, can be directly attributed to the reduced field strength and the speed of magnetic clouds arriving at Earth as a consequence of the anomalous expansion of CMEs due to the low ambient pressure in the heliosphere [*Gopalswamy et al*., 2015a, 2015b].

The strongest geomagnetic storm of the studied period occurred on 17 March 2013 near the equinox. Its main phase initiated after a clear sudden commencement, lasted for almost 12 h, and was followed by a long recovery phase (~6 days). This geomagnetic storm was accompanied by the strongest FD (5.1%) recorded during the entire studied period. These two events are associated with a quite fast (1063 km/s) halo CME ejected in the sequence of a moderately strong solar flare (M1.1 class) on 15 March 2013. However, this chain of events is not always so straightforward. There are situations where a geomagnetic storm (e.g., 19 February 2014, $Dst = -116$ nT) is not accompanied by a FD, and vice versa (e.g., 18 April 2014, FD = 4.5% without a geomagnetic storm). Additionally, there are geomagnetic storms that are not associated with any halo CME (on a time window of 3–4 days after the CME emergence), and, in turn, there are halo events that did not cause significant magnetic disturbances or FD. As a result, the *CR* series show low correlation with geomagnetic parameters (only for the *Smoothed* series, and with *Dst*, *r* is statistically significant; see Table 1). Still, most of the strong decreases in the CR flux took places during the epochs of geomagnetic disturbances of different length and strength (as is seen in Figures 3a and 3b and in Table S1). Also, as is shown in Table 1, there is (as expected) strong statistically significant correlation between the *Dst* and *COI H* original series which increases when the decadal trend is excluded from the *COI H* data (compare Table 1 (A and B) above diagonals).

The amount of the ozone (both in the total column and at specific level) in midlatitudinal atmosphere strongly depends on the rate of the atmospheric chemical reactions (which in turn depend on the atmospheric composition and temperature) and atmospheric dynamics (including QBO effect) [see *Randel and Cobb*, 1994]. However, it is still, to some degree, under a direct control by the solar UV flux. The atmospheric dynamics influence can explain the fact that the correlation between the *Smoothed* Mg II and $O_{3\ 10}$ series is positive during the eQBO phase (from 1 July 2012 to 30 June 2013, $r = 0.35$ p level = 0.19) and negative during the wQBO phase (from 1 July 2013 to 30 June 2014, $r = -0.35$, p level = 0.19)—also compare Figure 3c with Figures 3d–3f. However, for the entire 2 year period the correlation coefficients between these series are relatively high only for the *AC* series (Table 1). All the ozone series follow the quasi-27 day period of the UV variations caused by the solar rotation. However, the amplitude of ozone variations is not proportional to the amplitude of the UV variations. Besides, their month-to-month variations are not always in phase. The *CR* series (original and *Smoothed*) show anticorrelation with the ozone series (Table 1) which is statistically significant for the *Smoothed* $O_{3\ 10}$ and $O_{3\ tc}$ series. This is also seen in Figures 3b and 3d–3f: the epochs of strong FDs, i.e., less CR arriving to the Earth, like July and November 2012, June 2013, and March 2014, were also periods of highest levels of the ozone content. On the other side, these epochs were also characterized by higher levels of UV flux and frequent/strong geomagnetic storms.

5. Temperature and Pressure Modes and Their Covariation With Space Weather Parameters

As mentioned above, the raw data from the ground level CR detectors are very well anticorrelated with the atmospheric pressure. This is seen in Figures 4a and 4b where correlation coefficients between the original *T* and *gph* series at different pressure levels, and the raw (Figure 4a) and pressure-corrected (Figure 4b) *CR* data, are plotted as altitudinal profiles. The pressure correction removes correlation between the ground-measured pressure and *CR*; however, the correlation in the free atmosphere is still observed leaving possibilities to speculate on its origin. There could be three scenarios. The first one is that the CR particles affect different processes in the stratosphere and upper troposphere changing, as a result, temperature and pressure. The second scenario is that the thermodynamic conditions at those atmospheric levels affect productions of the secondary particles and, as a consequence, the ground-measured CR flux. The third option is that this correlation is artificially created by the corrections for the ground level pressure, since in the

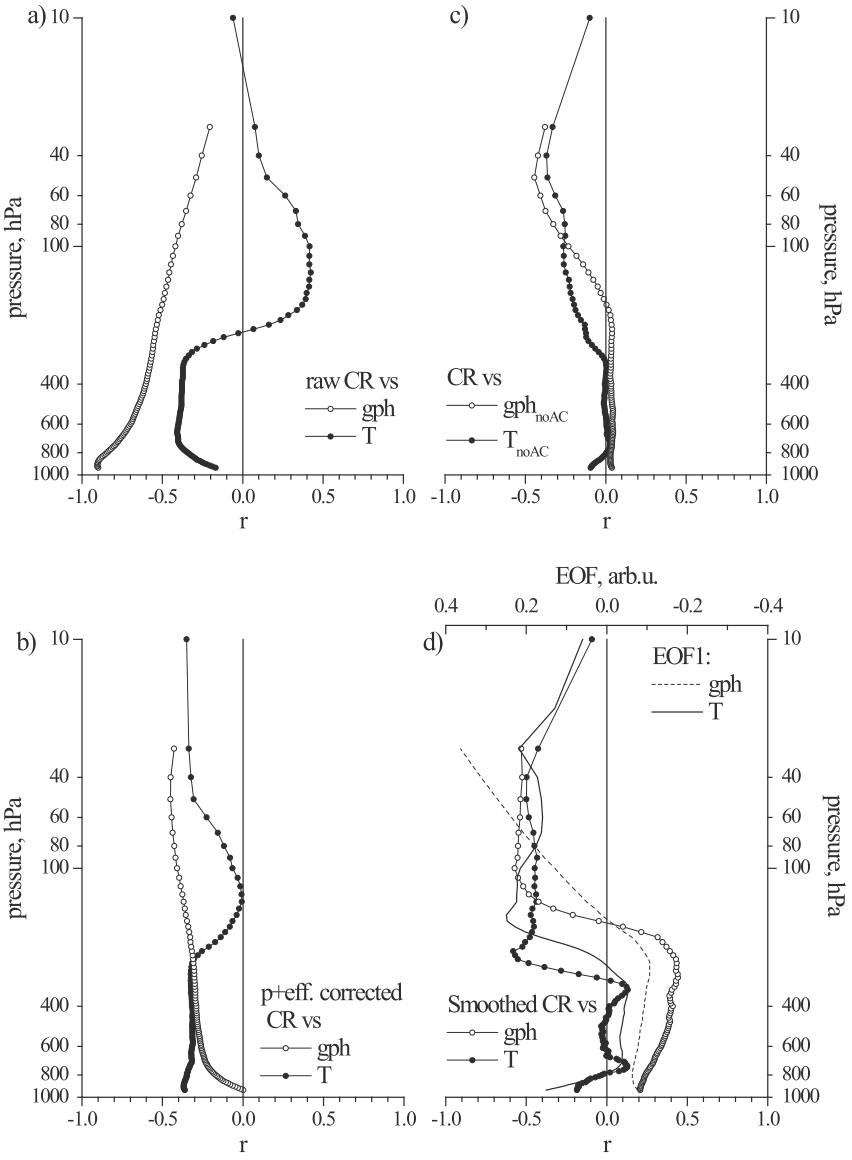

Figure 4. Altitudinal profiles of the correlation coefficients between the *T* (lines with filed circles) and *gph* (lines with open circles) series and *CR* series: (a) raw CR versus original *T* and *gph* series, (b) pressure and efficiency corrected CR versus original *T* and *gph* series, (c) *Smoothed* CR versus *noAC* T and *gph* series, and (d) *Smoothed* CR versus *Smoothed T* and *gph* series together with EOF1 from the PCA for the *Smoothed T* (solid line) and *gph* (dashed line) series. Please note that the top *X* axis (EOFs) is reversed.

troposphere pressure at different levels tends to correlate up to the ~100 hPa, and tropospheric temperature variations below ~300 hPa tends to anticorrelate with the ones above ~200 hPa.

The anticorrelation between the corrected *CR* and *T* and *gph* values in the free troposphere remains even after subtraction of the *AC* (Figure 4c). The correlation coefficients obtained for the *Smoothed* series show more complex variations with altitude (Figure 4d): significant anticorrelations between the *Smoothed T* and *CR* series exist only between ~250 hPa and ~30 hPa (tropopause and lower stratosphere region), i.e., about the atmospheric region where the main part of secondary cosmic rays is produced. This, in our mind, does not agree with the third hypothesis described above. The *Smoothed gph* and *CR* series show weak correlation at 400–200 hPa levels and anticorrelate above ~150 hPa level.

The spatial (EOF1) and temporal (PC1) components of the Modes 1 for the *T* and *gph* series are shown in Figures 4d and 5, correspondingly. The EOF1s have altitudinal distributions that resemble altitudinal

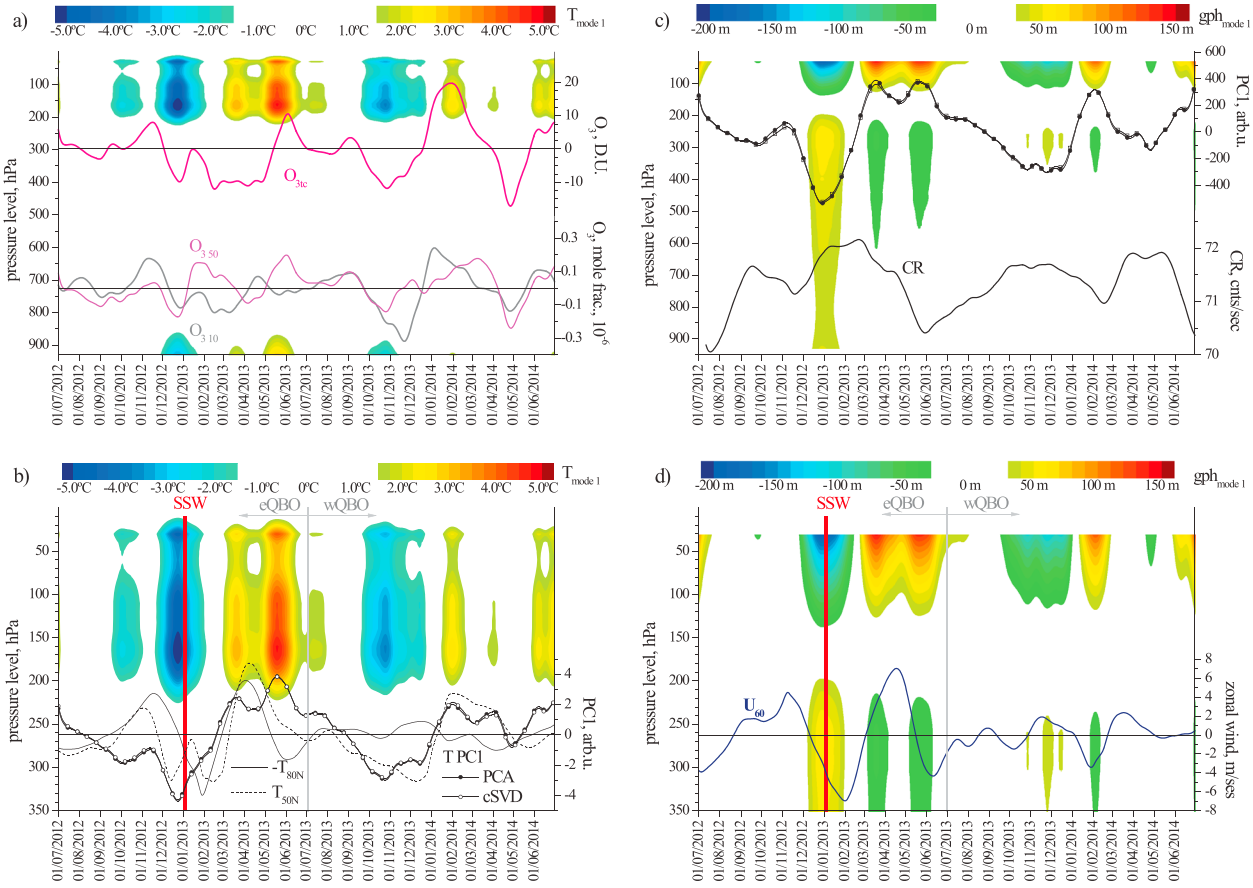

Figure 5. Reconstructed variations of the (a and b) *Smoothed* temperature and (c and d) *gph* series related to the Mode 1 (colors) together with ozone *Smoothed* series (Figure 5a, $O_{3\ tc}$—pink, $O_{3\ 10hPa}$—light grey, and $O_{3\ 50hPa}$—light pink), PC1s of the *Smoothed T* series (Figure 5b, lines with filed (PCA) and open (cSVD) circles), PC1 of T_{50N} (Figure 5b, solid line) and T_{80N} (Figure 5b, dashed line, sign reversed), PC1s for the *Smoothed gph* series (Figure 5c, lines with filed (PCA) and open (cSVD) squares), *Smoothed* series of CR (Figure 5c, thick line) and the mean zonally averaged zonal wind *U* at 60°N (Figure 5d, navy-blue line).In Figures 5b and 5d the vertical red lines mark SSW event and grey lines separate eQBO and wQBO epochs.

profiles of the correlation coefficients between the atmospheric parameters and the *CR*. The *T* and *gph* variations reconstructed using only first mode are shown in Figures 5a and 5b (*T*) and Figures 5c and 5d (*gph*) as color maps and as line with circles/squares (PC1s). Table 2 shows the explained variance fraction (in percent) for the first mode obtained by the PCA and cSVD analyses for the *T* and *gph* series. In case of cSVD two values are shown: an analogue of the PCA's explained variance fraction (*f*) and the explained squared covariance fractions (f_2). Mode 1 explains a significant part of the variability of the parental series: 67–79%. It is located in the upper troposphere-lower stratosphere region: from ~250 hPa up to ~10 hPa in case of *T* and from ~150 hPa up to at least 30 hPa in case of *gph*. For each of the analyzed PC1s the correlation coefficients with the *Smoothed* series of the space weather-related parameters are shown as well. As is seen in Figure 5b, temperature variations related to this mode follow changes of the zonal mean stratospheric temperature in the Northern Hemisphere (T_{50N} and T_{80N}) during the studied period. For example, during the strong SSW event in January 2013 (marked by the red vertical line) both T_{50N} and the stratospheric temperature above the Iberian Peninsula decrease. These distinctly antiphase variations with polar stratospheric temperature (T_{80N}) are seen only during the SSW2013 event.

The dependence of the Northern Hemisphere stratospheric conditions on the QBO phase was studied previously [e.g., *Chandran and Collins*, 2014; *Lu et al.*, 2014]. As it was shown, the eQBO often results in a weaker PV, warmer Arctic stratosphere, and more frequent SSW due to the way that planetary waves dissipate in the middle- and high-latitude Northern Hemisphere stratosphere (the so-called Holton and Tan mechanism [see, e.g., *Lu et al.*, 2008]). While the SSW events seriously affect conditions in the polar troposphere and stratosphere, their footprints are clearly seen at middle latitudes. The response of the

midlatitudinal atmosphere to the SSW depends on the type of the vortex disruption (splitting or displacement) and varies with longitude and from one event to another. In the case of the SSW2013, which started on 9 January 2013, the tropopause-lower stratosphere temperature and pressure above the IP (Figures 2 and 5) were significantly lower than the climatological means before the event (end of December 2012), increased to about the values of the climatological means during the main phase (first week of January 2013) and, finally, decreases again following the splitting of the PV (end of January–February 2013). These variations seen both in the sounding and satellite data (colors), in the zonal mean temperature data (solid lines), were discussed in other works [e.g., *Coy and Pawson*, 2015] and can be visualized using the National Centers for Environmental Prediction (NCEP)-NOAA and Environmental Research Laboratory (ERL)-NOAA online services. In fact, this kind of SSW-related variations seems to be more or less typical for the Northern Hemisphere lower stratosphere at ~40°N as was shown by, e.g., *Randel and Cobb* [1994] and *Hocke et al*. [2015]. Relations between the *gph* Mode 1 and the zonal wind speed/direction at 60°N are also QBO dependent (Figures 2 and 5): during the SSW2013 event (eQBO period) the strong easterlies (negative values of *U*) at 60°N were accompanied by the decreases of the pressure (*gph*) above the 150 hPa level. However, during the period of weak easterlies in January–February 2014 (wQBO) an increase of *gph* was observed.

The Mode 1 is well correlated with the ozone fraction at 50 hPa level, and the correlation with other ozone series is slightly lower (Table 2 and Figure 5a). The stratospheric temperature and ozone content are interdependent [*Mohanakumar*, 2008]. From one side, an increase/decrease of the ozone content results in an increase/decrease of the temperature due to the absorption of the UV solar radiations. On the other side, some chemical reactions of the ozone destruction are temperature dependent and an increase of the temperature in the presence, e.g., of a significant amount of NO_x species leads to a decrease of the ozone amount. Besides, both temperature and ozone content are affected by the air masses circulation. Nevertheless, while the correlation coefficients between the *Smoothed T* and $O_{3\ 50}$ series are similar for both the eQBO and wQBO periods (0.47, p value = 0.1 versus 0.50, p value = 0.05), the correlations between the *T* and other ozone series are high only during the wQBO phase (0 versus 0.65, p value = 0.01 for $O_{3\ 10}$ and 0 versus 0.60, p value = 0.04 for $O_{3\ tc}$). These differences are, probably, related to different atmospheric dynamics in the Northern Hemisphere at different altitudes under the eQBO/wQBO conditions (as was shown in, e.g., *Randel and Cobb* [1994] and *Lee and Smith* [2003]).

Mode 1 shows strong and significant anticorrelations with the *Smoothed CR* series (Table 2 and Figure 5c). Modes that covary with CR flux are obtained not only from the standard PCA but also when rotation is applied: in all cases the first modes (both for *T* and *gph*) are very similar to each other and correlate with the CR flux to the same degree. The periods of colder tropopause-lower stratosphere region with lower *gph* (lower pressure) coincide with the epochs of minima of the ozone content and maxima of the *CR* flux. The epochs of the minima in the *Smoothed CR* series (strong/frequent FDs) and the maxima of the ozone amount, in turn, coincides with the time periods of the warmer tropopause-lower stratosphere and higher *gph* (higher pressure) values. Also, the Mode 1 (anti)correlates with *Dst* (mostly, for *gph* PC1s, Table 2) but shows a not so clear correlation with *COI H* (showing differences between the variations of the GMF at global and regional scales) allowing us to assume that the anticorrelation with *Dst* arises from the similarities of the *Dst* (global-scale GMF variations) and *CR Smoothed* series (see Table 1 (B) below diagonal and Figures 3a and 3b), implying that at least at the considered time scales (weeks to months), CRs are ruled by global magnetospheric conditions more than by local variations in the magnetic field.

The covariability between the Mode 1 and the CR flux needs a more detailed analysis. On one hand, this dependence can result from the mentioned (section 1) local atmospheric effect (i.e., dependence of the ground measure CR flux on the atmospheric depth and/or pressure anomalies at the heights where secondary particles are generated) that is still present in the pressure-corrected ground-measured neutron monitor data. This possibility was discussed previously in, e.g., *Aplin et al*. [2005], *Sloan et al*. [2011], and *Harrison et al*. [2014]. On the other hand, the variations of the CR measured by neutron monitors over the whole globe used to be very well correlated (contrary to the stratospheric conditions), and the observed small differences, mainly in FD amplitude and the observation of ground level enhancements, can be attributed to their R_c or to the more or less favorable longitudinal position of a neutron monitor.

The covariability between the local conditions in the middle-latitude low atmosphere and CR flux can be also explained using the mechanism discussed in, e.g., *Mironova et al*. [2015]. This mechanism explains the

observed correlations between the stratospheric and tropospheric conditions in (mostly) arctic region and precipitations of energetic particles of different origin (energetic electron precipitations (EEPs), auroral electrons, SEP, CR, etc.) during the geomagnetic storms and other events. While the area of particle precipitations is limited to the auroral oval and polar upper atmosphere, the resulting changes of the atmospheric composition and temperature regime can be transferred to lower latitudes, even down to ~40°N, as was shown in simulations by *Rozanov et al*. [2012], through the atmospheric circulation. This transfer process can be affected by such hemispheric-scale events like SSW and QBO phase. It is worth to mention that the correlation of the polar stratospheric temperature with the level of the solar activity (which anticorrelated with the CR flux on the decadal time scale) in dependence on the QBO phase is known for a long time [see *Labitzke and Van Loon*, 1988; *Van Loon and Labitzke*, 1999; *Labitzke and Kunze*, 2012]. On the other side, the Iberian Peninsula, due to its midlatitudinal position, is under the influence of the dynamical processes in the tropical and subtropical stratosphere which were shown [*Garfinkel et al*., 2015, *Hood*, 2016] to respond to the solar activity variations in dependence with the QBO phase.

As to ozone, there is a number of studies showing that ozone content variations are related to the effect of SEP precipitating into the atmosphere of the polar (auroral) latitudes during geomagnetic storms [e.g., *Laštovička et al*., 1992; *Andersson et al*., 2014; *Verkhoglyadova et al*., 2014]. The CR and EEP particles affect the concentration of the nitrogen (NO_x) and hydrogen (HO_x) species leading to a decrease of the ozone content in the polar atmosphere. Since (especially during the SSW as shown in *Butler et al*. [2015]) the Northern Hemisphere midlatitude stratosphere and troposphere are under the strong influence of the PV, the NO_x and HO_x ions can be transported to the middle latitudes where they affect local ozone content (as is seen in our data). Other possibility is the direct influence of the CR flux variations on the local ozone content in midlatitudes and the (upper) stratospheric temperature through, e.g., the production of NO_x and HO_x [see, e.g., *Krivolutsky*, 2003; *Gray et al*., 2004].

The relatively high correlation coefficients among the CR, temperature, and ozone *Smoothed* series, especially for the higher pressure level (10 hPa), obtained in our analysis agree with both the "local influence" and "atmospheric dynamics" mechanisms. From one side, the time lag (1–2 weeks) observed between the temperature variations at 40°N and 50°N supports the "dynamical" hypothesis (transfer of the air masses from the polar to middle latitudes). Alternatively, the fact that the strongest correlation between the CR and temperature is observed at the altitudes of the secondary particles production gives a support to the hypothesis that the CR data are not fully corrected for the atmospheric effect. Same can be said about the ozone variations. In our opinion, an analysis of the relations between the atmospheric parameters and CR flux on a shorter time scale than the one used in this paper will help to discriminate between the local and dynamical effects.

6. Conclusions

The analysis of the regional (Iberian Peninsula) atmospheric parameters during a 2 year time interval (from July 2012 to June 2014) allowed us to extract modes of the temperature and *gph* (pressure) variations located mostly in the upper troposphere-lower stratosphere region, from ~250 hPa up to at least 30 hPa, that covary with some space weather parameters (e.g., cosmic ray).

The first mode of the regional atmospheric variability is related to the hemispheric-scale circulation driven, mostly, by the polar vortex conditions. The strength of the correlation between atmospheric conditions in the polar and middle latitudes during the studied time period seems to depend on the QBO phase which provides conditions for blocking or strengthening of the meridional circulation in the Northern Hemisphere stratosphere, though further studies are needed to confirm this QBO phase dependence.

The temperature variations associated to this mode correlate with the lower stratospheric ozone content and anticorrelate with cosmic rays flux variations. The *CR* series weakly correlates with geomagnetic parameters; nevertheless, all strong decreases in the CR flux took places during the epochs of geomagnetic disturbances of different length and strength.

The covariation of the atmospheric parameters and cosmic rays can be explained by one of the following mechanisms.

1. The first possible mechanism is related to the effect of the precipitating particles on the composition of the upper and middle atmosphere (in particular, on the NO_x and HO_x species) and, consequently, on

the ozone content in the polar regions and on the polar vortex conditions. Due to the coupling between the troposphere and stratosphere in the middle and high latitudes, variations in ozone content at high latitudes may affect atmosphere even at latitudes of ~40°N.

2. It is also possible that the observed covariability, at least partly, is due to the so-called atmospheric effect (dependence of the ground-measured neutron monitor data on the atmospheric temperature and pressure) which is not fully accounted for by the standard procedure of pressure corrections. This possibility is supported by the fact that the highest correlation coefficients between the CR and the Iberian *T* and *gph* series are obtained for the altitudes of ~100–200 hPa or ~12–16 km, the region where most of the secondary neutrons are produced.

The time scale of the variations analyzed in this paper (weeks to months) does not allow discriminating between these two mechanisms. The fact that the Mode 1 is of a hemispheric spatial scale cannot be used as a confirmation of the first mechanism: It is possible that changes in the polar atmosphere due to the precipitating particles are transferred to the middle latitudes and, in turn, affect local production of the secondary CR particles resulting in the variations of the locally measured ground level CR flux.

Glossary

AC/*noAC* series	annual cycle series/series without annual cycle
CME	coronal mass ejection
CR	cosmic ray
cSVD	coupled singular value decomposition
Dst	geomagnetic "disturbance storm time" index
EEP	energetic electron precipitations
EOF	empirical orthogonal function
FD	Forbush decrease
GMF	geomagnetic field
gph	geopotential height
MERRA	Modern-Era Retrospective Analysis for Research and Applications
Mg II	composite series of the solar UV radiation
NMDB	Neutron Monitor Database
O_3	ozone
PC	principal component
PCA	principal component analysis
PV	polar vortex
QBO	quasi-biennial oscillation
SEP	solar energetic particles
SSW	sudden stratospheric warming
STL	seasonal-trend decomposition with LOESS
T	temperature
UV	ultraviolet

Acknowledgments
Anna Morozova was supported by the postdoc from the Fundação para a Ciência e a Tecnologia (FCT) scholarship SFRH/BPD/74812/2010. Juan José Blanco was partially supported through the projects CCG2014/EXP-013 funded by the Alcalá University and ESP2013-48346-C02-1R funded by Ministerio de Economía y Competitividad. CITEUC is funded by National Funds through FCT—Foundation for Science and Technology (project UID/Multi/00611/2013) and FEDER—European Regional Development Fund through COMPETE 2020—Operational Programme Competitiveness and Internationalization (project POCI-01-0145-FEDER-006922). Sounding data were obtained through the GRA database http://www.ncdc.noaa.gov/data-access/weather-balloon/integrated-global-radiosonde-archive and University of Wyoming, College of Engineering, Department of Atmospheric Science http://weather.uwyo.edu/upperair/sounding.html. Zonally averaged stratospheric temperature and zonal wind data were downloaded from the MERRA websites http://gmao.gsfc.nasa.gov/research/merra/ and http://acdb-ext.gsfc.nasa.gov/Data_services/met/ann_data.html. We acknowledge the use of the area-averaged data on the stratospheric temperature and ozone from AIRS Science Team/Joao Texeira, 2012, last updated 2013: AIRX3STD v006. NASA/GSFC, Greenbelt, MD, USA, NASA Goddard Earth Sciences Data and Information Services Center (GES DISC). Accessed at 10.5067/AQUA/AIRS/DATA301. The data were obtained through Giovanni online data system, developed and maintained by the NASA GES DISC http://giovanni.sci.gsfc.nasa.gov/giovanni. Visualization of variations of stratospheric parameters is available at NCEP-NOAA (http://www.cpc.ncep.noaa.gov/products/stratosphere/temperature/) and ERL-NOAA (http://www.esrl.noaa.gov/psd/data/composites/day/) websites. The data on the QBO phases are from the Department of Earth Sciences of the Freie Universität Berlin http://www.geo.fu-berlin.de/met/ag/strat/produkte/qbo. Cosmic ray flux data are available from NMDB website http://www.nmdb.eu/nest/search.php or from http://www.calmanm.es. Geomagnetic data measured by the GAOUC are available by request (pribeiro@ci.uc.pt); the hourly values for the *X*, *Y*, and *Z* components from 2007 to 2014 can be also found at https://doi.pangaea.de/10.1594/PANGAEA.863008. We acknowledge the use of the *Dst* index from the Kyoto World Data Center http://wdc.kugi.

References

Andersson, M. E., P. T. Verronen, C. J. Rodger, M. A. Clilverd, and A. Seppälä (2014), Missing driver in the Sun–Earth connection from energetic electron precipitation impacts mesospheric ozone, *Nat. Commun.*, *5*, 5197, doi:10.1038/ncomms6197.

Andrade, C., and J. Corte-Real (2016), Assessment of the spatial distribution of continental-oceanic climate indices in the Iberian Peninsula, *Int. J. Climatol.*, *37*, 36–45, doi:10.1002/joc.4685.

Aplin, K. L., R. G. Harrison, and A. J. Bennett (2005), Effect of the troposphere on surface neutron counter measurements, *Adv. Space Res.*, *35*, 1484–1491.

Atmosphere, U.S. (1976), US Standard Atmosphere, National Oceanic and Atmospheric Administration.

Balachandran, N. K., and D. Rind (1995), Modeling the effects of UV variability and the QBO on the troposphere-stratosphere system. Part I: The middle atmosphere, *J. Clim.*, *8*(8), 2058–2079.

Baldwin, M. P., M. Dameris, and T. G. Shepherd (2007), How will the stratosphere affect climate change?, *Science*, *316*, 1576–1577.

Bazilevskaya, G. A. (2000), Observations of variability in cosmic rays, *Space Sci. Rev.*, *94*, 25–38.

Bazilevskaya, G. A., et al. (2008), Cosmic ray induced ion production in the atmosphere, *Space Sci. Rev.*, *137*(1–4), 149–173.

Bjornsson, H., and S. A. Venegas (1997), A manual for EOF and SVD analyses of climatic data, McGill University, *CCGCR Rep. 97-1*.

kyoto-u.ac.jp/dstae/index.html. The Mg II data are from Institute of Environmental Physics, University of Bremen http://www.iup.uni-bremen.de/gome/gomemgii.html. Solar and solar wind data are from SOHO/LASO database http://cdaw.gsfc.nasa.gov/CME_list, SOHO/EPHIN database http://www2.physik.uni-kiel.de/soho/phpeph/ephin.htm, OMNI database http://cdaweb.gsfc.nasa.gov/istp_public/, and GOES database ftp://ftp.ngdc.noaa.gov/STP/space-weather/solar-data/solar-features/solar-flares/x-rays/goes. We acknowledge the mission scientists and principal investigators who provided the data used in this research. The authors are grateful to the anonymous reviewers for their support and useful comments.

Braga, C. R., A. Dal Lago, T. Kuwabara, N. J. Schuch, and K. Munakata (2013), Temperature effect correction for the cosmic ray muon data observed at the Brazilian Southern Space Observatory in São Martinho da Serra, *J. Phys. Conf. Ser.*, *409*, 012138, doi:10.1088/1742-6596/409/1/012138.

Butler, A. H., D. J. Seidel, S. C. Hardiman, N. Butchart, T. Birner, and A. Match (2015), Defining sudden stratospheric warmings, *Bull. Am. Meteorol. Soc.*, *96*(11), 1913–1928.

De Castro, M., J. Martín-Vide, and S. Alonso (2005), The climate of Spain: Past, present and scenarios for the 21st century—A preliminary general assessment of the impacts in Spain due to the effects of climate change, Spanish Ministry of Environment, Madrid, 162.

Carslaw, K. (2009), Atmospheric physics: Cosmic rays, clouds and climate, *Nature*, *460*(7253), 332–333, doi:10.1038/460332a.

Chandran, A., and R. L. Collins (2014), Stratospheric sudden warming effects on winds and temperature in the middle atmosphere at middle and low latitudes: A study using WACCM, *Ann. Geophys.*, *32*(7), 859–874, doi:10.5194/angeo-32-859-2014.

Clem, J. M., and L. I. Dorman (2000), Neutron monitor response function, *Space Sci. Rev.*, *93*(1–2), 335–359.

Cleveland, R. B., W. S. Cleveland, J. E. McRae, and I. Terpenning (1990), STL: A seasonal-trend decomposition procedure based on LOESS, *J. Off. Stat.*, *6*, 3–73.

Cleveland, W. S. (1979), Robust locally weighted regression and smoothing scatterplots, *J. Am. Stat. Assoc.*, *74*(368), 829–836.

Cleveland, W. S., and S. J. Devlin (1988), Locally weighted regression: An approach to regression analysis by local fitting, *J. Am. Stat. Assoc.*, *83*(403), 596–610, doi:10.2307/2289282.

Coy, L., and S. Pawson (2015), The major stratospheric sudden warming of January 2013: Analyses and forecasts in the GEOS-5 data assimilation system, *Mon. Weather Rev.*, *143*(2), 491–510.

Danilov, A.D., and J. Laštovička (2001), Effects of geomagnetic storms on the ionosphere and atmosphere, Int. *Int. J. Geomagn. Aeron.*, *2*(3), 209–224.

Dorman, L. I. (2009), *Cosmic Rays in Magnetospheres of the Earth and Other Planets*, *Astrophys. Space Sci. Library*, vol. 358, Springer Sci. and Business Media B.V., Dordrecht, Netherlands.

Ebisuzaki, W. (1997), A method to estimate the statistical significance of a correlation when the data are serially correlated, *J. Clim.*, *10*(9), 2147–2153.

Ern, M., et al. (2016), Satellite observations of middle atmosphere gravity wave activity and dissipation during recent stratospheric warmings, *Atmos. Chem. Phys. Discuss.*, *16*, 9983–10019, doi:10.5194/acp-2016-276.

Forbush, S. E. (1938), On world-wide changes in cosmic-ray intensity, *Phys. Rev.*, *54*, 975–988, doi:10.1103/PhysRev.54.975.

Garfinkel, C. I., V. Silverman, N. Harnik, C. Haspel, and Y. Riz (2015), Stratospheric response to intraseasonal changes in incoming solar radiation, *J. Geophys. Res. Atmos.*, *120*, 7648–7660, doi:10.1002/2015JD023244.

Goncharenko, L., and S. R. Zhang (2008), Ionospheric signatures of sudden stratospheric warming: Ion temperature at middle latitude, *Geophys. Res. Lett.*, *35*, L21103, doi:10.1029/2008GL035684.

Gopalswamy, N., S. Akiyama, S. Yashiro, H. Xie, P. Makela, and G. Michalek (2015a), The mild space weather in solar cycle 24, arXiv:1508.01603v1 [astro-ph.SR.]

Gopalswamy, N., S. Yashiro, and S. Akiyama (2015b), Kinematic and energetic properties of the 2012 March 12 polar coronal mass ejection, *Astrophys. J.*, *809*(1), 106.

Gray, L. J., S. A. Crooks, C. Pascoe, S. Sparrow, and M. Palmer (2004), Solar and QBO influences on the timing of stratospheric sudden warmings, *J. Atmos. Sci.*, *61*, 2777–2796.

Guo, J., X. Feng, J. M. Forbes, J. Lei, J. Zhang, and C. Tan (2010), On the relationship between thermosphere density and solar wind parameters during intense geomagnetic storms, *J. Geophys. Res.*, *115*, A12335, doi:10.1029/2010JA015971.

Haigh, J. D. (2003), The effects of solar variability on the Earth's climate, *Philos. Trans. R. Soc., A*, *361*(1802), 95–111.

Hannachi, A., I. T. Jolliffe, and D. B. Stephenson (2007), Empirical orthogonal functions and related techniques in atmospheric science: A review, *Int. J. Climatol.*, *27*(9), 1119–1152.

Harrison, R. G., K. A. Nicoll, and K. L. Aplin (2014), Vertical profile measurements of lower troposphere ionisation, *J. Atmos. Sol. Terr. Phys.*, *119*, 203–210.

Hocke, K., M. Lainer, and A. Schanz (2015), Composite analysis of a major sudden stratospheric warming, *Ann. Geophys.*, *33*(6), 783–788.

Hood, L. L. (2004), Effects of solar UV variability on the stratosphere, in *Solar Variability and Its Effects on Climate*, *Geophys. Monogr. Ser.*, vol. 141, edited by J. Pap and P. Fox, pp. 283–303, AGU, Washington, D. C., 283–303.

Hood, L. L. (2016), Lagged response of tropical tropospheric temperature to solar ultraviolet variations on intraseasonal time scales, *Geophys. Res. Lett.*, *43*, 4066–4075, doi:10.1002/2016GL068855.

Knipp, D., L. Kilcommons, L. Hunt, M. Mlynczak, V. Pilipenko, B. Bowman, Y. Deng, and K. Drake (2013), Thermospheric damping response to sheath-enhanced geospace storms, *Geophys. Res. Lett.*, *40*, 1263–1267, doi:10.1002/grl.50197.

Krivolutsky, A. A. (2003), History of cosmic ray influence on ozone layer-key steps, *Adv. Space Res.*, *31*(9), 2127–2138.

Kudela, K., and R. Brenkus (2004), Cosmic ray decreases and geomagnetic activity: List of events 1982–2002, *J. Atmos. Sol. Terr. Phys.*, *66*(13), 1121–1126.

Künsch, H. R. (1989), The jackknife and the bootstrap for general stationary observations, *Ann. Stat.*, *17*, 1217–1241.

Labitzke, K., and M. Kunze (2012), Interactions between the stratosphere, the Sun and the QBO during the northern summer, *J. Atmos. Sol. Terr. Phys.*, *75-76*, 141–146.

Labitzke, K., and H. Van Loon (1988), Associations between the 11-year solar cycle, the QBO and the atmosphere. Part I: The troposphere and stratosphere in the northern hemisphere in winter, *J. Atmos. Terr. Phys.*, *50*(3), 197–206.

Lahiri, S. N. (1999), Theoretical comparisons of block bootstrap methods, *Ann. Stat.*, *27*, 386–404.

Laštovička, J. (1996), Effects of geomagnetic storms in the lower ionosphere, middle atmosphere and troposphere, *J. Atmos. Terr. Phys.*, *58*(7), 831–843.

Laštovička, J., J. Bremer, and M. Gil (1992), Ozone response to major geomagnetic storms, *Ann. Geophys.*, *10*(9), 683–689.

Lee, H., and A. K. Smith (2003), Simulation of the combined effects of solar cycle, quasi-biennial oscillation, and volcanic forcing on stratospheric ozone changes in recent decades, *J. Geophys. Res.*, *108*(D2), 4049, doi:10.1029/2001JD001503.

Le Mouël, J. L., E. Blanter, M. Shnirman, and V. Courtillot (2009), Evidence for solar forcing in variability of temperatures and pressures in Europe, *J. Atmos. Sol. Terr. Phys.*, *71*(12), 1309–1321.

Limpasuvan, V., D. W. Thompson, and D. L. Hartmann (2004), The life cycle of the Northern Hemisphere sudden stratospheric warmings, *J. Clim.*, *17*(13), 2584–2596.

Limpasuvan, V., D. L. Hartmann, D. W. Thompson, K. Jeev, and Y. L. Yung (2005), Stratosphere-troposphere evolution during polar vortex intensification, *J. Geophys. Res.*, *110*, D24101, doi:10.1029/2005JD006302.

Lockwood, M. (2012), Solar influence on global and regional climates, *Surv. Geophys.*, *33*(3–4), 503–534.

Lu, H., M. P. Baldwin, L. J. Gray, and M. J. Jarvis (2008), Decadal-scale changes in the effect of the QBO on the northern stratospheric polar vortex, *J. Geophys. Res.*, *113*, D10114, doi:10.1029/2007JD009647.
Lu, H., T. J. Bracegirdle, T. Phillips, A. Bushell, and L. Gray (2014), Mechanisms for the Holton-Tan relationship and its decadal variation, *J. Geophys. Res. Atmos.*, *119*, 2811–2830, doi:10.1002/2013JD021352.
Maruyama, T., and M. Nakamura (2007), Conditions for intense ionospheric storms expanding to lower midlatitudes, *J. Geophys. Res.*, *112*, A05310, doi:10.1029/2006JA012226.
Medina, J., et al. (2013), Castilla-La Mancha neutron monitor, *Nucl. Instrum. Methods Phys. Res., Sect. A*, *727*, 97–103.
Mironova, I. A., K. L. Aplin, F. Arnold, G. A. Bazilevskaya, R. G. Harrison, A. A. Krivolutsky, K. A. Nicoll, E. V. Rozanov, E. Turunen, and I. G. Usoskin (2015), Energetic particle influence on the Earth's atmosphere, *Space Sci. Rev.*, *194*, 1–96, doi:10.1007/s11214-015-0185-4.
Mlynczak, M. G., L. A. Hunt, B. T. Marshall, J. M. Russell III, C. J. Mertens, R. E. Thompson, and L. L. Gordley (2015), A combined solar and geomagnetic index for thermospheric climate, *Geophys. Res. Lett.*, *42*, 3677–3682, doi:10.1002/2015GL064038.
Mohanakumar, K. (2008), Stratosphere troposphere interactions: An introduction, Springer Science & Business Media.
Morozova, A. L., and T. V. Barlyaeva (2016), The role of climatic forcings in variations of Portuguese temperature: A comparison of spectral and statistical methods, *J. Atmos. Sol. Terr. Phys.*, *149C*, 240–257, doi:10.1016/j.jastp.2016.02.006.
Nakamura, K. (Particle Data Group) (2010), Review of particle physics, *J. Phys. G Nucl. Part Phys.*, *37*, 075021, doi:10.1088/0954-3899/37/7A/075021.
Oh, S. Y., Y. Yi, and Y. H. Kim (2008), Globally nonsimultaneous Forbush decrease events and their implications, *J. Geophys. Res.*, *113*, AO1103, doi:10.1029/2007JA012333.
Osprey, S., et al. (2009), Sudden stratospheric warmings seen in MINOS deep underground muon data, *Geophys. Res. Lett.*, *36*, L05809, doi:10.1029/2008GL036359.
Pancheva, D., and P. Mukhtarov (2011), Stratospheric warmings: The atmosphere–ionosphere coupling paradigm, *J. Atmos. Sol. Terr. Phys.*, *73*(13), 1697–1702.
Randel, W. J., and J. B. Cobb (1994), Coherent variations of monthly mean total ozone and lower stratospheric temperature, *J. Geophys. Res.*, *99*(D3), 5433–5447.
Rozanov, E., M. Calisto, T. Egorova, T. Peter, and W. Schmutz (2012), Influence of the precipitating energetic particles on atmospheric chemistry and climate, *Surv. Geophys.*, *33*(3–4), 483–501.
Shlens, J. (2009), A tutorial on principal component analysis, Systems Neurobiology Laboratory, University of California at San Diego, version 3.01, 2009. [Available at http://snl.salk.edu/~shlens/pca.pdf.]
Sloan, T., G. A. Bazilevskaya, V. S. Makhmutov, Y. I. Stozhkov, A. K. Svirzhevskaya, and N. S. Svirzhevsky (2011), Ionization in the atmosphere, comparison between measurements and simulations, *Astrophys. Space Sci. Trans*, *7*, 29–33, doi:10.5194/astra-7-29-2011.
Snow, M., M. Weber, J. Machol, R. Viereck, and E. Richard (2014), Comparison of Magnesium II core-to-wing ratio observations during solar minimum 23/24, *J. Space Weather Space Clim.*, *4*, 6, doi:10.1051/swsc/2014001.
Sugiura, M., and T. Kamei (1991), Equatorial *Dst* index 1957–1986, IAGA bull., 40, IUGG, Paris.
Tinsley, B. A. (2008), The global atmospheric electric circuit and its effect on cloud microphysics, *Rep. Prog. Phys.*, *71*(6), 066801.
Tonev, P. T., and P. I. Y. Velinov (2015), Vertical coupling between troposphere and lower ionosphere by electric currents and fields at equatorial latitudes, *J. Atmos. Sol. Terr. Phys.*, *141*, 39–47, doi:10.1016/j.jastp.2015.10.012.
Tsagouri, I., A. Belehaki, G. Moraitis, and H. Mavromichalaki (2000), Positive and negative ionospheric disturbances at middle latitudes during geomagnetic storms, *Geophys. Res. Lett.*, *27*(21), 3579–3582, doi:10.1029/2000GL003743.
Verkhoglyadova, O. P., M. Butala, S. Wang, M. G. Mlynczak, L. A. Hunt, and G. P. Zank (2014), Effects of two large solar energetic particle events on middle atmosphere nighttime odd hydrogen and ozone content, *J. Geophys. Res. Space Physics*, *120*, 12–29, doi:10.1002/2014JA020609.
Van Loon, H., and K. Labitzke (1999), The signal of the 11-year solar cycle in the global stratosphere, *J. Atmos. Sol. Terr. Phys.*, *61*(1), 53–61.
Yiğit, E., P. K. Knížová, K. Georgieva, and W. Ward (2016), A review of vertical coupling in the atmosphere–ionosphere system: Effects of waves, sudden stratospheric warmings, space weather, and of solar activity, *J. Atmos. Sol. Terr. Phys.*, *141*, 1–12.